processed for fluorescence and immunofluorescence microscopy. During rapamycin treatment, nonfasting blood glucose level was monitored daily using samples obtained from the tail vein. To further determine the effects of rapamycin on glucose tolerance, intraperitoneal glucose tolerance test (IPGTT) was conducted before and at days 14 and 28 after treatment (41). In this test, mice were fasted for 6 h and then injected intraperitoneally with 2 g glucose in saline/kg body weight. Blood glucose levels were measured for 2 h at 30 min intervals. Moreover, to detect the change in insulin secretion after *in vivo* rapamycin treatment, plasma insulin levels were also measured by ELISA before and after the treatment (at days 0, 7, 14, 21, 28 and 35, n = 5 mice, each group).

Fluorescence microscopy and immunofluorescence microscopy

Pancreatic tissue samples for GFP examination were prepared as follows. To prevent artificial induction of autophagy during sample preparation, mice were anesthetized by diethyl ether and immediately fixed by transcardial perfusion through the left ventricle with 4% paraformaldehyde dissolved in 0.1 M Na-phosphate buffer (pH 7.4). Subsequently, the pancreas was removed and further fixed with the same fixative for another 4 h at room temperature, followed by treatment with 5% sucrose in PBS for 2 h and then with 15% sucrose solution for 4 h, finally with 30% sucrose solution overnight. Pancreatic tissue samples were embedded in Tissue-Tek OCT compound (Sakura Finetechnical Co., Tokyo, Japan) and stored at −80°C. The tissue samples were sectioned at 7 μm thickness with a cryostat, air-dried for 30 min at room temperature and then stored at −80°C until use. Fluorescence signals were analyzed by Biozero fluorescence microscopy (Keyence, Osaka, Japan) by measuring green fluorescence (excitation, 488 nm; emission, 530 nm).

For general histological examination, cryosections were stained with hematoxylin and eosin. Furthermore, for immunofluorescence microscopy, cryosections were prepared as described earlier. After rinsing with water for 5 min, the sections were blocked with 4% bovine serum albumin (BSA)–PBS for 10 min at room temperature. Subsequently, these sections were incubated with rabbit polyclonal anti-mouse insulin Ab (SC-9168; Santa Cruz Biotechnology, Santa Cruz, CA, USA) overnight at 4°C diluted in 1% BSA-TBS-Tween-20 (0.05% w/v), followed by incubation with Alexa fluor555 goat anti-mouse IgG (H+L) Ab (A21429; 1:1000 dilution; Invitrogen, Carlsbad, CA, USA) for 30 min at room temperature. Fluorescence signals were observed by Biozero fluorescence microscopy (Keyence). The fluorescence intensities of insulin and GFP-LC3 in treated islets were quantified using Fluor-Chem image analyzer (Bio-Rad Laboratories Inc., Hercules, CA, USA) and expressed in arbitrary units. The mean fluorescence intensities of insulin and GFP, expressed as mean ± standard deviation (SD), were determined in islets of five rapamycin-treated mice. To identify apoptotic β cells in the pancreas of mice, islet sections were stained with terminal deoxynucleotidyl transferase-mediated dUTP nick-end labeling (TUNEL) using Tumor TACS™ *In Situ* Apoptosis Detection Kit (catalog# 4815–30-K, Trevigen, Gaithersburg, MD, USA) following the instructions provided by the manufacturer.

Statistical analysis

Data were expressed as mean ± SD and analyzed using Excel for Windows software. Two samples were compared with the Student's *t*-test. The p values <0.05 denoted the presence of statistical significance.

Details of the mice used in these experiments, islet isolation to assess the effects of rapamycin treatment *in vitro* and western blot analysis are presented in the Supplementary Materials and Methods in the on line version of the journal.

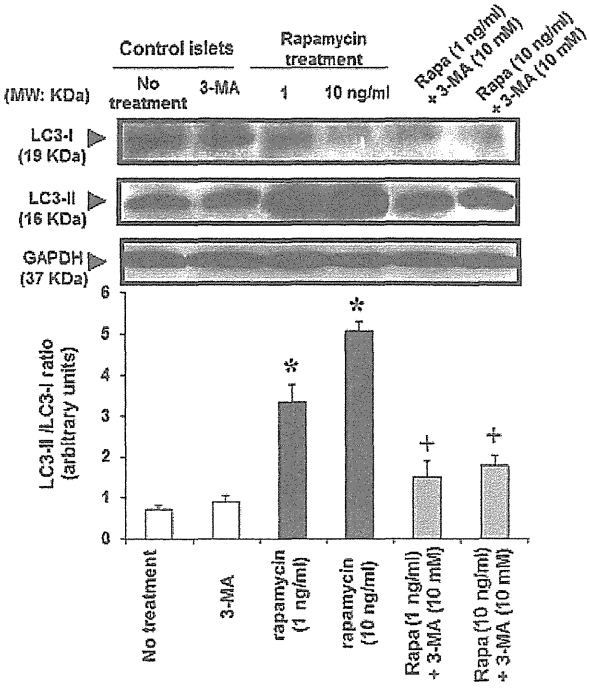

Figure 1: Changes in LC3-I and LC3-II protein expression levels in rapamycin-treated islets. LC3-I and LC3-II protein expression level were examined by western blot analysis. Protein samples extracted from either untreated islets, rapamycin-treated or rapamycin + 3-MA-treated islets were subjected to 15% SDS/PAGE and transferred onto PVDF membrane. Representative photographs are shown, together with mouse GAPDH levels as an internal control. Quantification of the intensity of the immunoreactive bands of both LC3-I and LC3-II, expressed in arbitrary units, was carried out using NIH Image J software. Results of densitometric analysis of immunoblots of LC3 in islets were expressed as the ratio of LC3-II to LC3-I. Data are mean ± SD of three independent experiments. $^{*}p < 0.05$, versus control islet; $^{+}p < 0.05$, versus rapamycin-treated islets.

Results

In vitro *overinduction of autophagy in pancreatic islets by rapamycin*

Control islets, including untreated islets and 3-MA-treated islets, showed similar levels of endogenous expression of LC3-II protein (Figure 1). Islets treated with 1 or 10 ng/mL of rapamycin showed the highest expression of LC3-II protein. The conversion of LC3-I (cytosolic form) to LC3-II (membrane-bound lapidated form) was detected by immunoblotting. The amounts of LC3-II protein were three- to fivefold higher in 1 and 10 ng/mL rapamycin-treated islets, respectively, as assessed by the LC3-II/LC3-I ratio (Figure 1). The rapamycin-induced increase in LC3-II level suggests increased autophagy flux. Quantification of LC3-II band intensities showed that blockade of autophagy by 3-MA prevented the accumulation of LC3-II protein in islets treated with 1 or 10 ng/mL of rapamycin. With regard

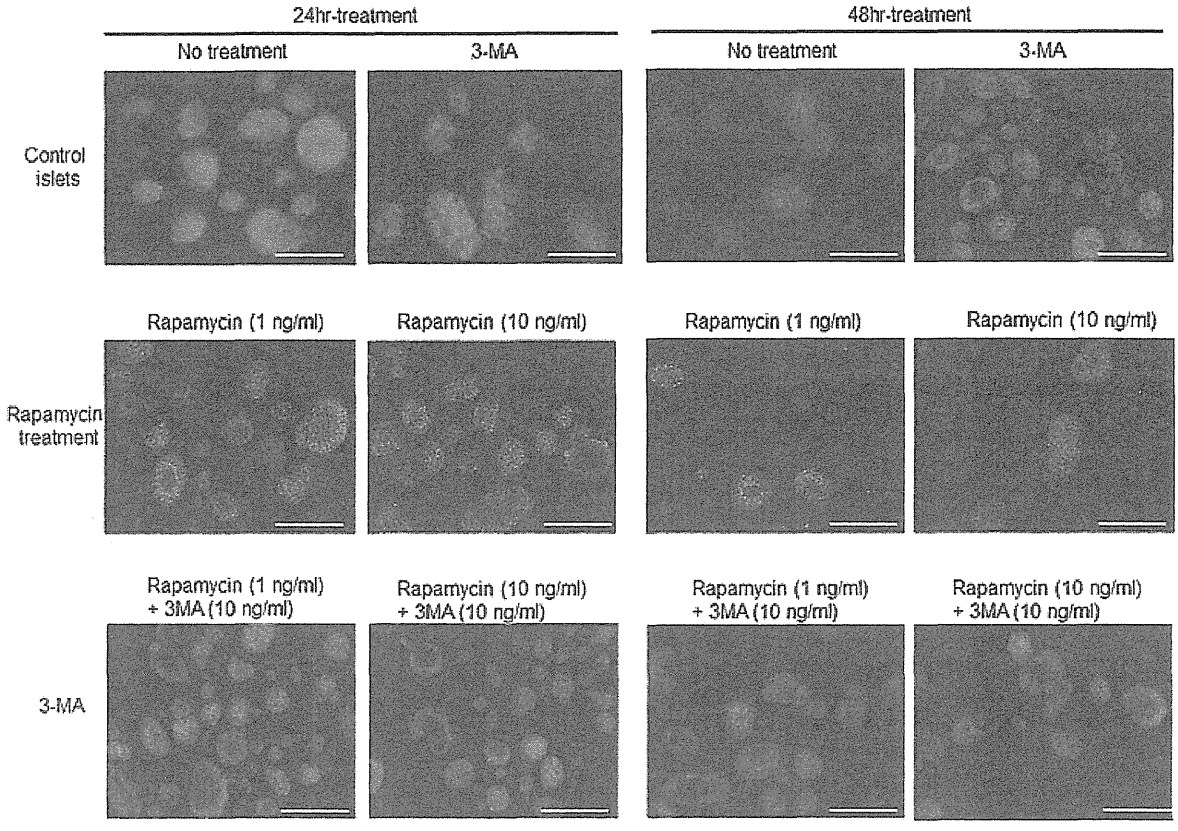

Figure 2: *In vitro* overinduction of autophagy in response to rapamycin treatment. Fresh islets samples were prepared from GFP-LC3 transgenic mice, and then incubated for either 24 or 48 h in the absence or presence of rapamycin. In 3-MA blocking, fresh islets were incubated in the presence of both rapamycin and 3-MA. After treatment, the GFP signal was detected by fluorescence microscopy. Bars = 100 μm.

to the conversion of LC3-I to LC3-II, the LC3-II/LC3-I ratio was significantly reduced in islets treated with rapamycin-plus-10 mM 3-MA compared with that of islets treated with rapamycin alone (Figure 1).

As shown in the top panels of Figure 2, a diffuse GFP-LC3 signal was detected in the control islets, with few GFP puncture dots. After 24 h incubation with 1 or 10 ng/mL of rapamycin, the number of GFP-LC3 dots was markedly increased; most dots were detected as cup- or ring-shaped structures (left middle panels, Figure 2). These findings indicate overinduction of autophagy in rapamycin-treated islets. In contrast, the fluorescence level of GFP-LC3 signal in rapamycin-treated islets in the presence of 10 mM 3-MA was diffuse and returned to the basal level of autophagy in control islets (left bottom panels, Figure 2). After 48 h incubation with rapamycin, many large ring- or cup-shaped structures were identified by fluorescence microscopy (right middle panels, Figure 2). Furthermore, the fluorescence signals of GFP-LC3 in rapamycin-plus-3-MA-treated islets continued to show diffuse distribution and persisted at the basal level of autophagy seen in the control islets (right bottom panels, Figure 2). Taken together, the results indicate that the blocking effects of 3-MA were persistent rather than transient.

Rapamycin-related overinduction of autophagy in islet cells reduces islet viability

To examine the effect of overinduction of autophagy by rapamycin on islet viability, we performed MTS assay (Figure 3) and fluorescence labeling with TMRE and 7-AAD (Figure 4). Viability under treatment with 3-MA alone was similar to the control islets (Figure 3). Treatment with 1 and 10 ng/mL rapamycin resulted in approximately 43% and 51% reduction of viability, respectively (Figure 3). In contrast, 3-MA ameliorated the effect of rapamycin on islet viability (Figure 3).

To further determine the effect of rapamycin on islet viability, islet cells were stained with TMRE or 7-AAD and assessed by FACS analysis. 3-MA had no significant effect on islet viability (control, 80.5 ± 4.5%; 3-MA, 80.4 ± 5.5%) and the percentages of dead cells (i.e. 7-AAD-positive cells; control, 4.7 ± 3.5%; 3-MA, 3.9 ± 4.3%). Rapamycin significantly decreased the proportion of TMRE-positive cells

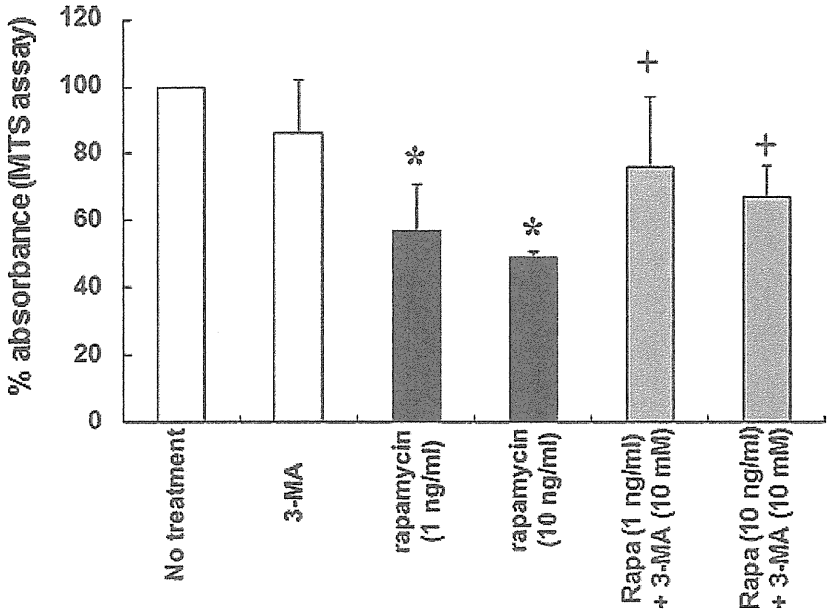

Figure 3: *In vitro* viability assessments of rapamycin-treated islet by MTS assay. Control islets, rapamycin-treated and rapamycin-3-MA-treated islets were assessed for islet viability. Data are mean ± SD of five independent islets preparations. The% absorbance of treated islets was expressed relative to absorbance of control islets, which was set at 100%. *$p < 0.05$, versus control islets; $^{+}p < 0.05$, versus rapamycin-treated islets.

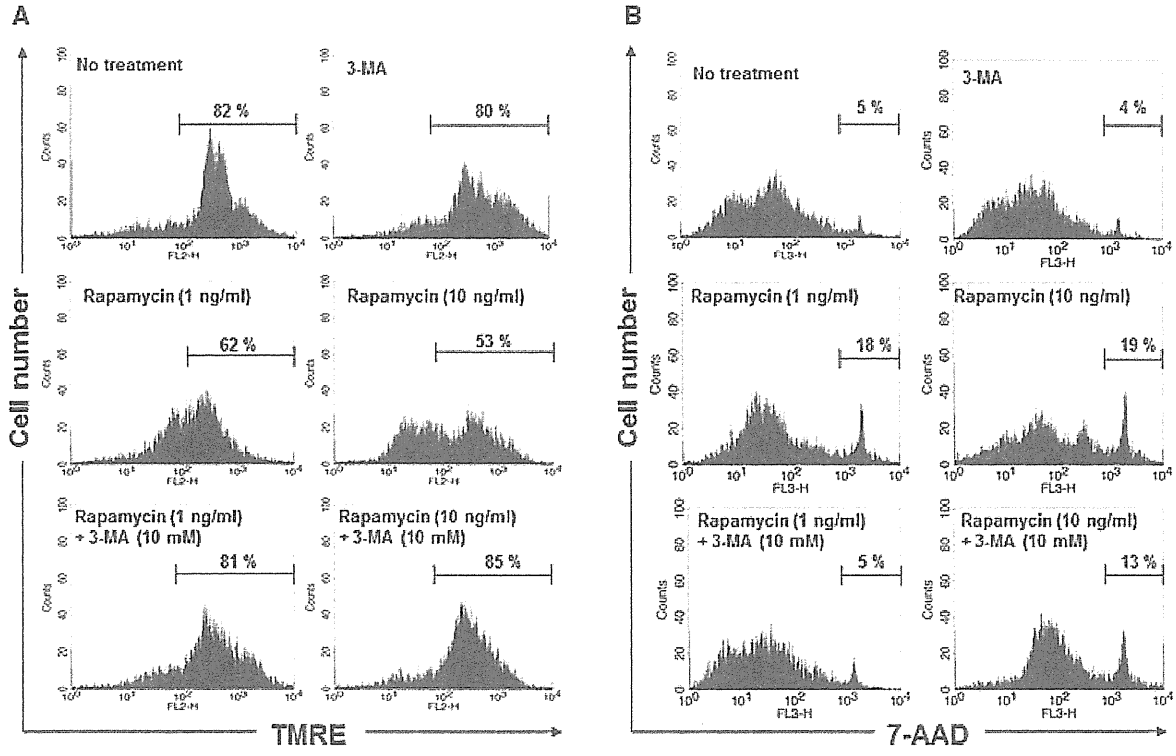

Figure 4: *In vitro* analysis of the cytotoxic effect of rapamycin and upregulation of autophagy. Islets were incubated with either 1 or 10 ng/mL of rapamycin for 24 h to overinduce autophagy. In blocking assay, islets were cultured with rapamycin in the presence of 10 mM 3-MA. After dispersion of mice islets into single cell suspensions, cells were stained with TMRE or 7-AAD. (A) Pancreatic β cells were analyzed for the relative percentage of apoptotic or nonapoptotic cells by TMRE. (B) Dead cells represented 7-AAD-positive cells. Data are representative of five independent experiments using different mice islets reparations.

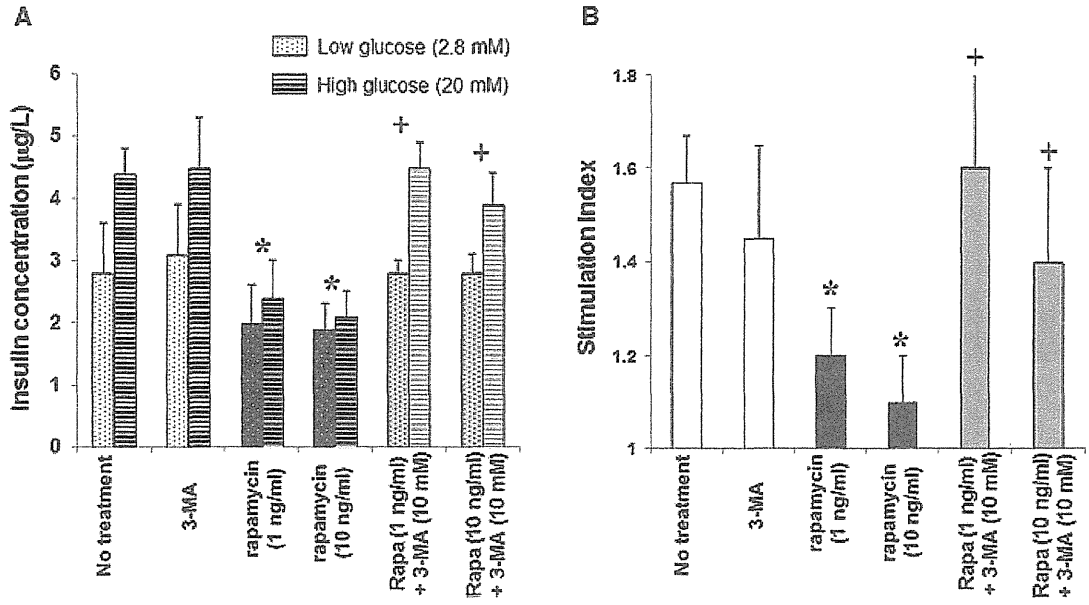

Figure 5: *In vitro* assessment of the effect of rapamycin on insulin production from islets. Production of insulin was assessed by static glucose challenge and the results expressed as both (A) blood insulin concentration and (B) stimulation index (SI). Data are mean ± SD of five independent islet preparations. *$p < 0.05$, compared with the control; $^{+}p < 0.05$, compared with rapamycin alone.

(1 ng/mL of rapamycin, 62.4 ± 6.7%; 10 ng/mL of rapamycin, 52.1 ± 6.1%; compared with the control, $p < 0.05$), and significantly increased the percentage of 7-AAD-positive cells (1 ng/mL of rapamycin, 17.7 ± 7.6%; 10 ng/mL of rapamycin, 18.7 ± 6.7%; compared with the control islets, $p < 0.05$). The addition of 3-MA to rapamycin-treated islets ameliorated the effects of the latter on the percentages of both viable and dead cells (Figures 4A and B). Taken together, these data suggest that rapamycin-induced overinduction of autophagy negatively affects islet viability and mitochondrial integrity, and that these effects are blocked by 3-MA.

Rapamycin reduces islet insulin production

Islet insulin potency was assessed by static glucose challenge *in vitro*. In control islets, insulin was secreted at 4.4–4.5 μg/L under high glucose medium (Figure 5A). In contrast, insulin secretion under high glucose medium was significantly inhibited in rapamycin-treated islets and treatment with rapamycin elicited approximately 45–53% reduction in insulin concentration (Figure 5A). We also analyzed islets' insulin production using the SI. The SI of untreated control islets was 1.57 ± 0.13 (Figure 5B). 3-MA did not have a significant effect on insulin production compared with the control islets. However, rapamycin significantly reduced the SI (1 ng/mL of rapamycin, 1.20 ± 0.1; 10 ng/mL of rapamycin, 1.11 ± 0.12; $p < 0.05$, each, compared with the control islets). The addition of 3-MA to rapamycin-treated islets markedly improved both insulin production and SI. Especially, insulin production showed complete recovery in islet treated with 1 ng/mL of rapamycin and 10 mM of 3-MA (Figures 5A and B). These results indicate that rapamycin elicits not only overinduction of autophagy but also reduction of both islet viability and *in vitro* insulin function.

Effect of nutrient starvation on autophagy in GFP-LC3 transgenic mice

To confirm the beneficial effects of 3-MA on induction of autophagy in the intact animal, we used GFP-LC3 transgenic mice and examined autophagy in 3-MA-treated transgenic mice under starvation. In the control GFP-LC3 transgenic mice, few GFP-LC3 dots were observed in pancreatic acinar cells and such dots were relatively small. In the pancreatic islets, no GFP dots were detected and these islets were clearly stained for insulin (top panels, Figure 6). The GFP-LC3 structures appeared 24 h after starvation as large cup-shaped structures in both islet and acinar cells. To validate these findings, we examined both muscle (as an example of nonessential tissue) and brain (as an essential tissue) tissues by fluorescence microscopy. As shown in Figure 7(A), no GFP dots were observed in the extensor digitorum longus muscles before starvation, however, GFP-LC3 dots appeared after 24 h starvation in muscle tissues (Figure 7B). On the other hand, in brain samples, including the cerebral cortex and medulla oblongata, no GFP-LC3 structures could be detected in spite of 24 h starvation (Figures 7D and F). In addition, islets starved for 24 h stained faintly for insulin (middle panels, Figure 6). The mean insulin staining intensity of starved islets was markedly reduced compared with that of untreated control islets, although the difference in insulin intensity was

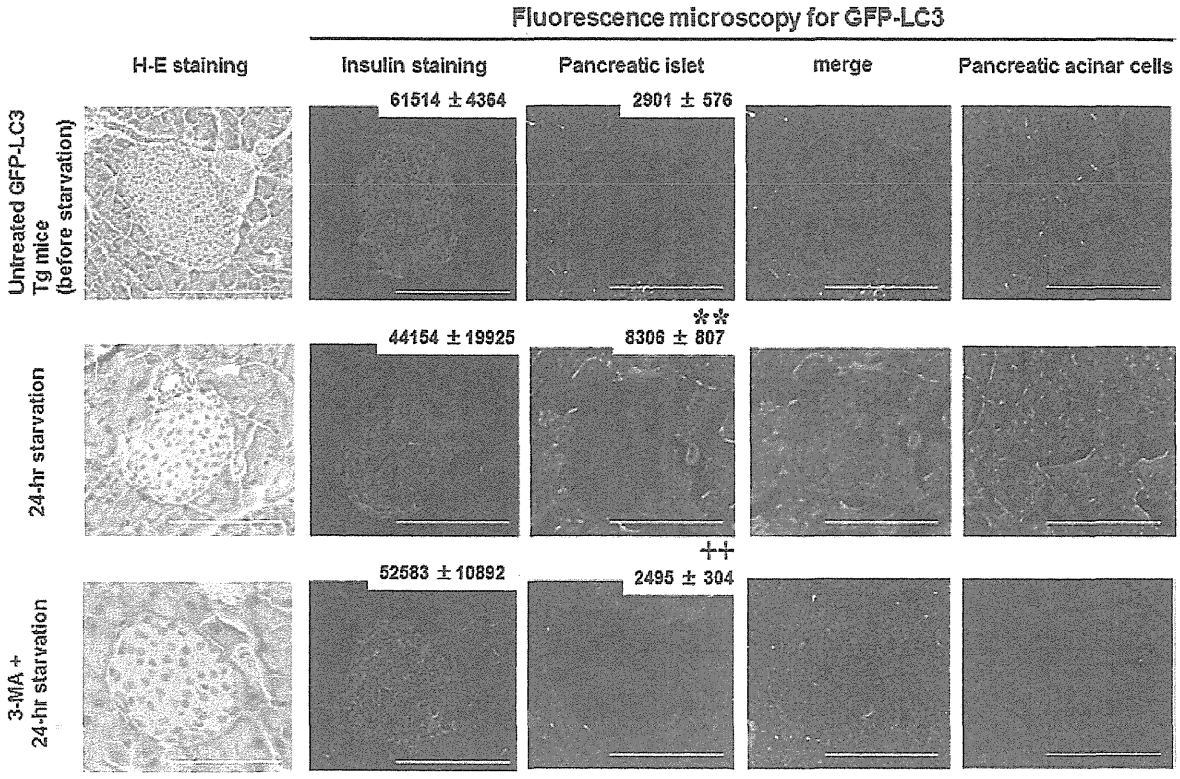

Figure 6: Starvation induced autophagy in pancreatic islets and acinar cells of GFP-LC3 transgenic mice. Representative images of islets stained with H&E and for insulin after 24 h starvation. Representative GFP images of pancreatic islets, acinar cells and merged microphotographs of GFP images and insulin staining. Numbers in the right upper corner of the photographs represent the mean ± SD intensity of GFP and insulin staining, expressed in arbitrary units, of five different islets. $^{**}p < 0.01$, compared with the control; $^{++}p < 0.01$, compared with 24 h starvation. Bars = 100 μm.

not significant (control, 61 514 ± 4364; starvation, 44 154 ± 19 925). The mean fluorescence intensity of GFP-dots was significantly higher in starved islets than untreated control islets (control, 2901 ± 576; starvation, 8306 ± 807; $p < 0.01$). The merged images of GFP signals of LC3 dots and the adjacent islets stained for insulin are shown in Figure 6. The merged microphotographs also showed weaker insulin intensity in starved islets compared with the control islets. The use of 3-MA during 24 h starvation ameliorated the effect of 24 h starvation as evident by the appearance—diffuse and few fluorescence signals of GFP-LC3 dots—and by the return of GFP fluorescence intensity in islets. Furthermore, the recovered islets stained positive for insulin and the intensity of such staining was similar to the control islets, as judged by both the mean staining intensity and the merged microphotographs (lower panels, Figure 6).

Effect of rapamycin on autophagy in GFP-LC3 transgenic mice

Finally, we assessed the effects of rapamycin on autophagy and insulin production in transgenic mice *in vivo*. For this purpose, the mice were treated with 0.2 mg/kg of rapamycin intraperitoneally daily for 1, 2, 3, 4 or 5 weeks. After 1 week of such treatment, small but few dots appeared in both islets and acinar cells, however, no significant difference was observed in the pancreas of rapamycin-treated mice and rapamycin-plus-3-MA (10 mM)-treated mice (top panels, Figures 8A and B). After 2, 3, 4 and 5 weeks of rapamycin treatment, a marked increase in the density of GFP-LC3 dots was observed and these dots appeared as ring- or cup-shaped structures in both islets and acinar cells (Figures 8A and B). The GFP fluorescence intensity was higher in 1-week treated islets than in untreated control islets, although no significant large GFP dots were observed (Figures 6 and 8A). After 2, 3, 4 and 5 weeks of treatment, the GFP fluorescence intensity in the treated islets was significantly up-regulated compared with those in control and 1-week treated islets. In spite of overinduction of autophagy in rapamycin-treated islets, the mean intensities of insulin in 2-, 3-, 4- and 5-week rapamycin-treated islets were significantly lower than the control untreated islets (Figure 8A). Interestingly, 3-MA ameliorated the changes in immunofluorescence, including GFP-LC3 dots and insulin staining intensity, which reflects rapamycin-induced overinduction of autophagy (Figure 8B). The merged

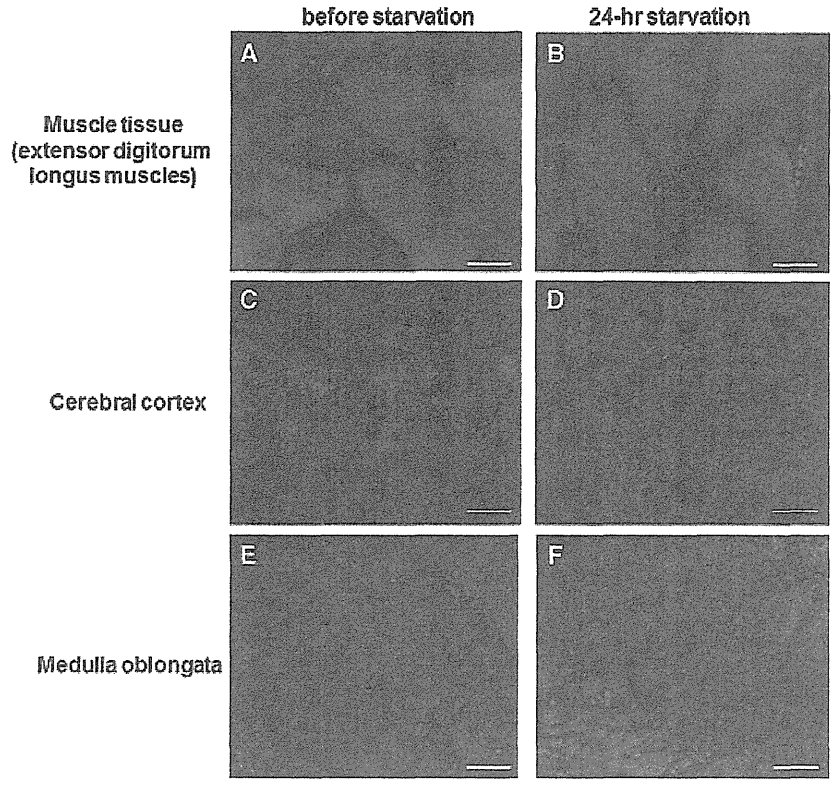

Figure 7: Starvation induced autophagy in muscle tissues, but not in brain. GFP images of transverse sections of extensor digitorum longus muscle (A) before starvation and (B) after starvation. GFP images of the cerebral cortex (C) before starvation and (D) after starvation. GFP images of medulla oblongata (E) before starvation and (F) after starvation. Bars = 10 μm.

microphotographs also demonstrated reduced insulin intensity in rapamycin-treated islets and that the degenerative change showed significant recovery in islets of the rapamycin-plus-3-MA group. TUNEL-positive cells were detected in 2-, 3-, 4- and 5-week rapamycin treated islets. In contrast, no such cells were observed in islets treated with rapamycin-plus-3-MA. Taken together, these *in vivo* findings correlated well with the *in vitro* data, including islet insulin potency and TMRE viability assay.

To further determine the effects of rapamycin on islet function in mice, we measured nonfasting blood glucose and plasma insulin concentrations. Rapamycin had no significant effect on nonfasting blood glucose levels, and near-normoglycemia was noted in mice treated with rapamycin alone and in those treated with rapamycin-plus-3-MA (Figures 9A and B). At days 14, 21, 28 and 35 after treatment, plasma insulin levels were higher in rapamycin-plus-3-MA-treated mice than in rapamycin-treated mice. Especially, plasma insulin concentration at day 14 in rapamycin-treated mice was significantly lower than in rapamycin-plus-3-MA-treated mice (Figures 9C and D). All other differences in insulin concentration were not significant between the two groups. Interestingly, in IPGTT performed at day 14, the blood glucose level of mice treated with rapamycin alone was significantly higher than in those treated with rapamycin-plus-3-MA at 15, 30, 60, 90 and 120 min after injection of glucose. Thus, rapamycin elicited a diabetic glucose pattern in mice (Figure 9E). In contrast, in the same test performed at day 28, the blood glucose levels of rapamycin-treated mice were similar to those of mice treated with rapamycin-plus-3-MA, and the pattern of blood glucose after injection was also similar between the two groups (Figure 9F). Taken together, rapamycin treatment resulted in impairment of *in vivo* glucose tolerance until 2 weeks after treatment and this abnormality was reversed by co-administration of 3-MA. It is possible that this abnormality of glucose tolerance represents physiological adjustment, such as reduction of insulin resistance at day 28. Further analysis of this phenomenon requires *in vivo* experiments of long-term rapamycin treatment.

Discussion

Rapamycin has deleterious effects on islet β cell based on the blockade of VEGF-mediated survival pathways and inhibition of β-cell proliferation and by induction of apoptosis (20,34,42). Accordingly, we raised the question of whether rapamycin in islet transplantation is a friend or a foe. In this study, we focused on the effect of rapamycin on autophagy and evaluated the direct effect of rapamycin on islet β cells. Using various techniques, the results demonstrated for the first time that rapamycin at therapeutically used concentrations, overinduced autophagy both *in vitro* and *in vivo* and that this effect on islet β cells impaired both islet viability and insulin potency.

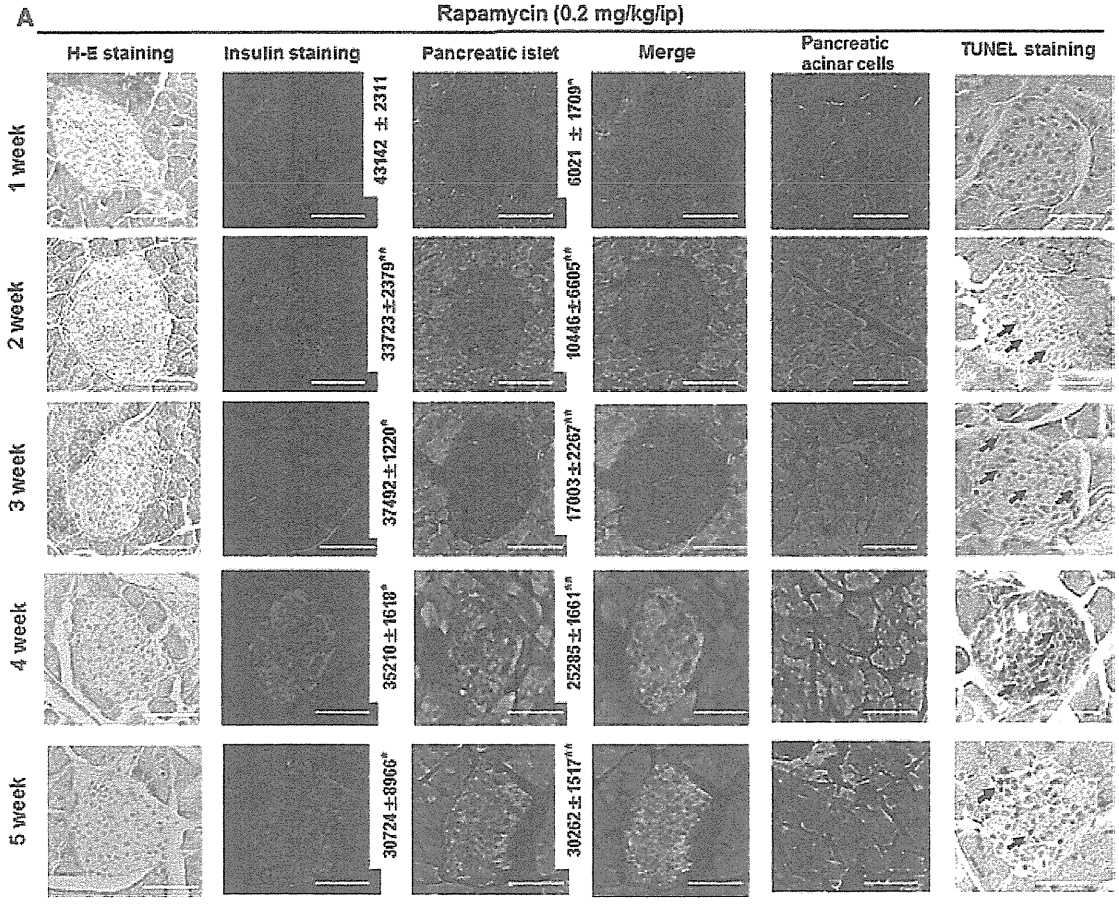

Figure 8: Upregulation of autophagy in rapamycin-treated GFP-LC3 transgenic mice. Representative images of islets stained with H&E, GFP images of pancreatic islets and acinar cells, images of islets stained for insulin and images of TUNEL staining after the indicated period of treatment. Also shown are the merged microphotographs of GFP images and insulin staining. Numbers in the right upper corner of the photographs represent the mean ± SD intensity of GFP and insulin staining, expressed in arbitrary units, of five different islets. *$p < 0.05$, compared with the control; **$p < 0.01$, compared with the control; $^{++}p < 0.01$, compared with rapamycin alone. Images were obtained from GFP-LC3 transgenic mice treated with (A) 0.2 mg/kg/i.p. rapamycin alone and (B) 0.2 mg/kg/i.p. rapamycin-plus-10 mM 3-MA. Bars = 100 μm.

Autophagy is the degradation of redundant or faulty cell components (1–4,12). Recent studies have described a link between diabetes and autophagy (43,44). Two groups independently reported the findings of increased apoptosis and reduced proliferation of β cells with resultant reduction in β-cell mass in β-cell-specific autophagy-deficient mice ($Atg7^{f/f}$: RIP-Cre mice; Refs. 43,44). These studies indicated that basal autophagy is indispensable for the maintenance of normal islet architecture, such as mitochondria and function of β cells (43,44).

As shown in Figure 1 and immunoblot analyses reported by others (36,44–46), endogenous LC3-II expression was detected in cell lysates from pancreatic islets and a low level of constitutive autophagy (here referred to as "basal autophagy") was present in normal control islets. Our results also showed that rapamycin resulted in overinduction of autophagy in islets with consequent impairment of insulin function, both *in vitro* and *in vivo*. These results suggest that overinduction of autophagy by rapamycin in islet β cells negatively affects insulin function by modulating cell death through accelerated self-digestion and degradation of essential cellular components. Based on the effect of rapamycin on islet β cells, it is possible that excessive digestion of various types of cellular structures, including insulin granules, mitochondria and endoplasmic reticulum membranes takes place in autophagic vacuoles, because this structure lacks stringent substrate specificity, which is different from that used by the ubiquitin–proteasome system (47); in other words, any structure in the cytosol could become a substrate for autophagy (43,44). This may explain the significantly low insulin production capacity of *in vitro*

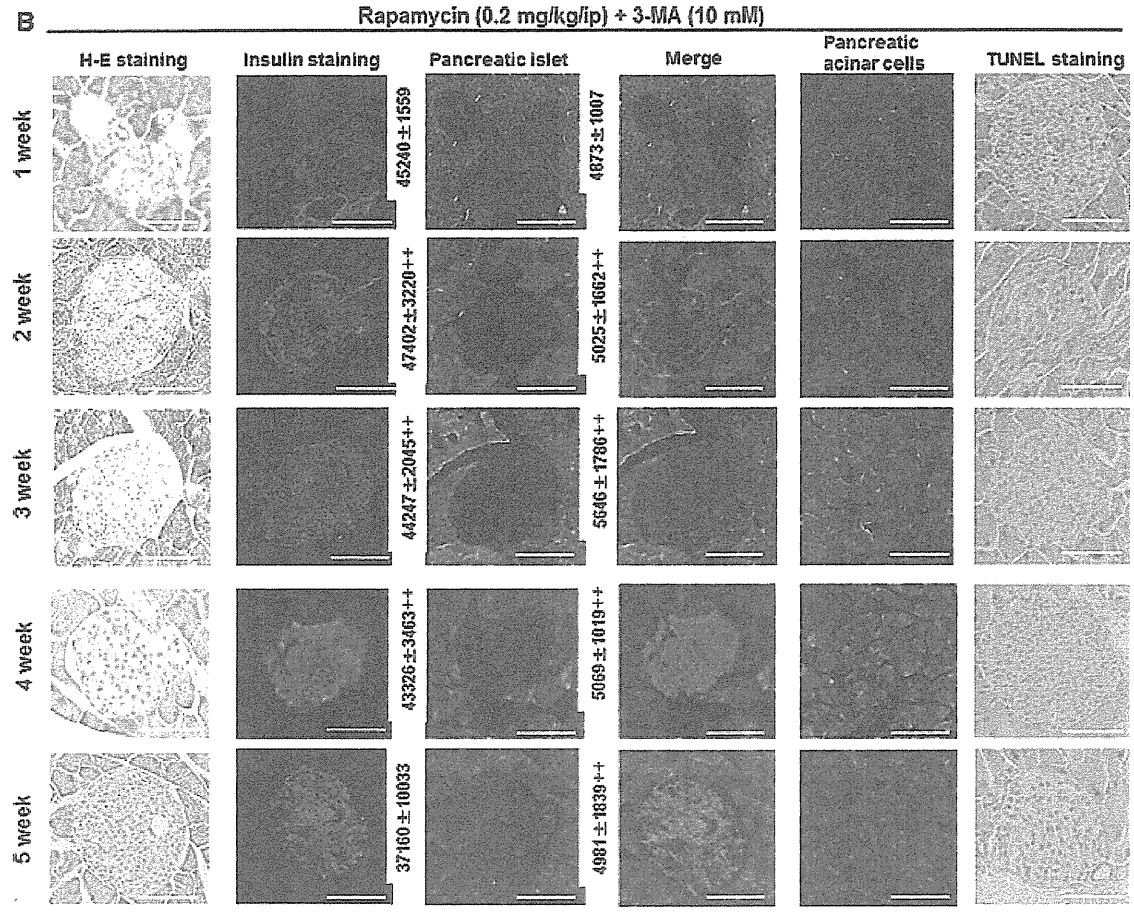

Figure 8: Continued.

rapamycin-treated islet β cells, the significant reduction of insulin staining intensity in islets of rapamycin-treated mice and the marked impairment of glucose tolerance assessed by IPGTT (Figures 5, 8A and 9E). Based on these results, we speculate that the main etiology of progressive dysfunction of transplanted islets is reduced insulin production related to rapamycin treatment and the related overinduction of autophagy.

Although the protective role of basal autophagy on pancreatic β-cell function has been proposed in loss-of-function studies on Atg/genes (43,44,48), accelerated autophagy seems to be involved in certain types of cell death (2,49–51). For this reason, we evaluated β-cell apoptosis by TMRE staining and TUNEL, and dead cells by 7-AAD. Figures 4A and B showed that rapamycin increased the percentages of apoptotic β cells and 7-AAD-positive dead islet cells. Furthermore, the TUNEL-positive apoptotic cells were observed in islets of rapamycin-treated mice and these apoptotic cells disappeared after the administration of 3-MA. These findings seem to indicate the existence of crosstalk between autophagy and apoptosis and various links between autophagy and cell death, which may occur in a hierarchial or independent fashion (52–55). In this regard, Masini et al. (48) reported that exposure of nondiabetic islets to high concentrations of free fatty acid resulted in accumulation of autophagic vacuoles. Together with enhanced β-cell death, which was associated with decreased LAMP2 expression. These results suggest that accelerated autophagy may contribute to β-cell death under special conditions, such as rapamycin treatment.

The upregulation of autophagy after rapamycin treatment resulted in a significant impairment of β-cell insulin function, and this effect may contribute to islet graft dysfunction observed in islet recipients. We also demonstrated that 3-MA ameliorated rapamycin-related β-cell dysfunction both *in vitro* and *in vivo*. Thus, this new modulator of autophagy, such as 3-MA, should be tested further clinically, and better therapeutic agents with specific autophagic activity need to be developed for the prevention and treatment of islet graft dysfunction.

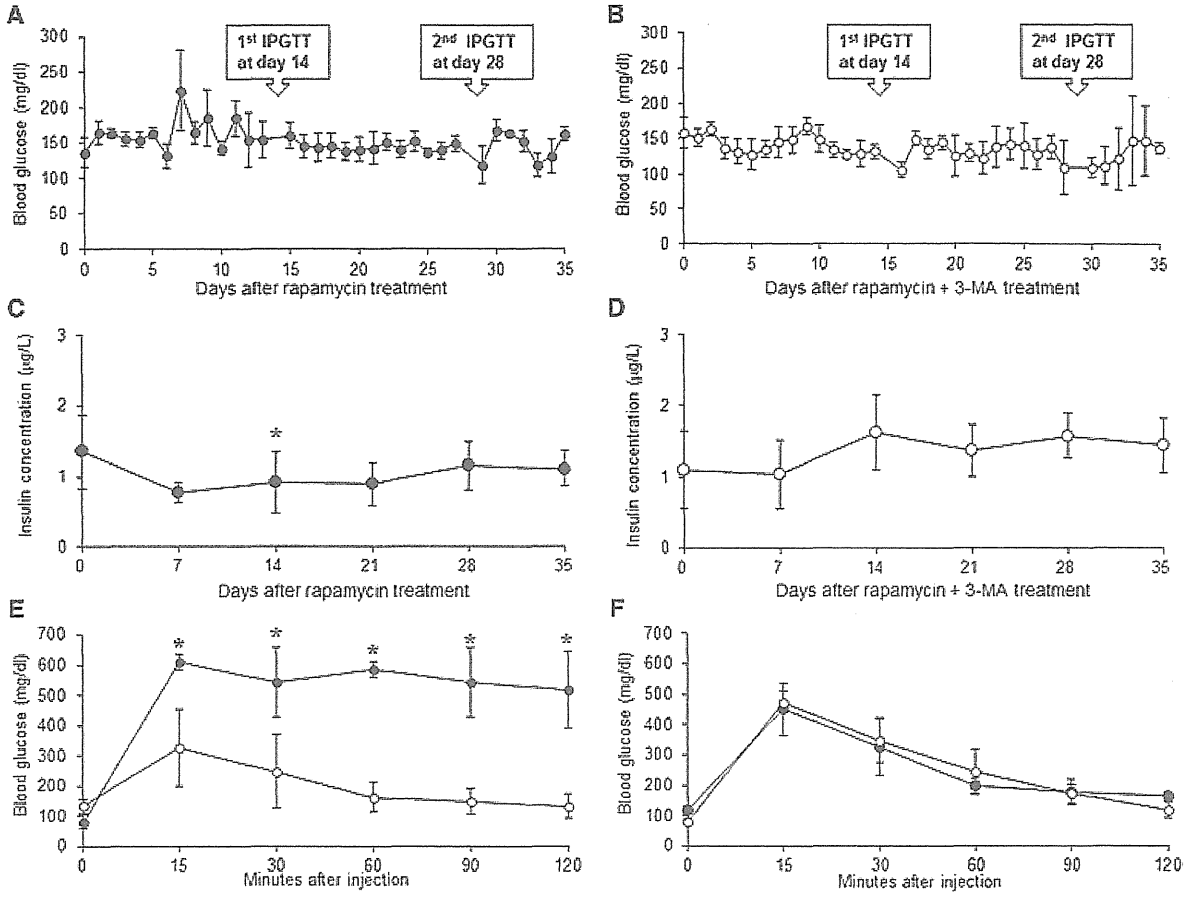

Figure 9: Nonfasting blood glucose and plasma insulin concentrations after treatment and glucose tolerance test at days 14 and 28. (A) Blood glucose level of GFP-LC3 transgenic mice treated with 0.2 mg/kg/i.p. rapamycin alone. (B) Blood glucose level of GFP-LC3 transgenic mice treated with 0.2 mg/kg/i.p. rapamycin-plus-10 mM 3-MA. (C) Plasma insulin concentration of mice treated with 0.2 mg/kg/i.p. rapamycin alone. (D) Plasma insulin concentration of mice treated with 0.2 mg/kg/i.p. rapamycin-plus-10 mM 3-MA. (E) Glucose tolerance test after treatment at day 14. (F) Glucose tolerance test after treatment at day 28. Closed circles: data of mice treated with 0.2 mg/kg/i.p. rapamycin alone; open circles: data of mice treated with 0.2 mg/kg/i.p. rapamycin-plus-10 mM 3-MA. Data are mean ± SD of five mice in each treatment group.

Acknowledgments

The authors thank Dr. F.G. Issa (www.word-medex.com.au) for the careful reading and editing of the manuscript. We also thank Dr. N. Kawaguchi and Prof. N. Matsuura (Osaka University) for their help in the execution of this project and the valuable suggestions.

Funding source: This work was supported by a grant from the Ministry of Education, Sports and Culture of Japan to M. T. (No. 22591520) and by Kobayashi Foundation for Cancer Research to M. T.

Disclosure

The authors of this manuscript have no conflicts of interest to disclose as described by the *American Journal of Transplantation.*

References

1. Levine B, Klionsky DJ. Development by self-digestion: Molecular mechanisms and biological functions of autophagy. Dev Cell 2004; 6: 463–477.
2. Levine B, Kroemer G. Autophagy in the pathogenesis of disease. Cell 2008; 132: 27–42.
3. Mizushima N, Yoshimori T, Levine B. Methods in mammalian autophagy research. Cell 2010; 140: 313–326.
4. Kuma A, Hatano M, Matsui M, et al. The role of autophagy during the early neonatal starvation period. Nature 2004; 432: 1032–1036.
5. Ravikumar B, Vacher C, Berger Z, et al. Inhibition of mTOR induces autophagy and reduces toxicity of polyglutamine expansions in fly and mouse models of Huntington disease. Nat Genet 2004; 36: 585–595.
6. Hara T, Nakamura K, Matsui M, et al. Suppression of basal autophagy in neural cells causes neurodegenerative disease in mice. Nature 2006; 441: 885–889.

7. Komatsu M, Waguri S, Chiba T, et al. Loss of autophagy in the central nervous system causes neurodegeneration in mice. Nature 2006; 441: 880–884.
8. Levine B. Cell biology: Autophagy and cancer. Nature 2007; 446: 745–747.
9. Nakai A, Yamaguchi O, Takeda T, et al. The role of autophagy in cardiomyocytes in the basal state and in response to hemodynamic stress. Nat Med 2007; 13: 619–624.
10. Virgin HW, Levine B. Autophagy genes in immunity. Nat Immunol 2009; 10: 461–470.
11. Levine B, Mizushima N, Virgin HW. Autophagy in immunity and inflammation. Nature 2011; 469:323–335.
12. Mizushima N. The pleiotropic role of autophagy: From protein metabolism to bactericide. Cell Death Differ 2005; 12: 1535–1541.
13. Abraham RT. Mammalian target of rapamycin: Immunosuppressive drugs uncover a novel pathway of cytokine receptor signaling. Curr Opin Immunol 1998; 10: 330–336.
14. Augustine JJ, Bodziak KA, Hricik DE. Use of sirolimus in solid organ transplantation. Drugs 2007; 67: 369–391.
15. Kirken RA, Wang YL. Molecular actions of sirolimus: Sirolimus and mTor. Transplant Proc 2003; 35 (Suppl 3): 227S-230S.
16. Hay N, Sonenberg N. Upstream and downstream of mTOR. Genes Dev 2004; 18: 1926–1945.
17. Schmelzle T, Hall MN. TOR, a central controller of cell growth. Cell 2000; 103: 253–262.
18. Shapiro AM, Lakey JR, Ryan EA, et al. Islet transplantation in seven patients with type 1 diabetes mellitus using a glucocorticoid-free immunosuppressive regimen. N Engl J Med 2000; 343: 230–238.
19. Ryan EA, Lakey JR, Rajotte RV, et al. Clinical outcomes and insulin secretion after islet transplantation with the Edmonton protocol. Diabetes 2001; 50: 710–719.
20. Markmann JF, Deng S, Huang X, et al. Insulin independence following isolated islet transplantation and single islet infusions. Ann Surg 2003; 237: 741–749.
21. Froud T, Ricordi C, Baidal DA, et al. Islet transplantation in type 1 diabetes mellitus using cultured islets and steroid-free immunosuppression: Miami experience. Am J Transplant 2005; 5: 2037–2046.
22. Hering BJ, Wijkstrom M. Sirolimus and islet transplants. Transplant Proc 2003; 35 (Suppl 3): 187S–190S.
23. Li Y, Li XC, Zheng XX, et al. Blocking both signal 1 and signal 2 of T-cell activation prevents apoptosis of alloreactive T cells and induction of peripheral allograft tolerance. Nat Med 1999; 5: 1298–1302.
24. Battaglia M, Stabilini A, Draghici E, et al. Induction of tolerance in type 1 diabetes via both CD4+CD25+ T regulatory cells and T regulatory type 1 cells. Diabetes 2006; 55: 1571–1580.
25. Ryan EA, Paty BW, Senior PA, et al. Five-year follow-up after clinical islet transplantation. Diabetes 2005; 54: 2060–2069.
26. Desai NM, Goss JA, Deng S, et al. Elevated portal vein drug levels of sirolimus and tacrolimus in islet transplant recipients: Local immunosuppression or islet toxicity? Transplantation 2003; 76: 1623–1625.
27. Ricordi C, Zeng YJ, Alejandro R, et al. *In vivo* effect of FK506 on human pancreatic islets. Transplantation 1991; 52: 519–522.
28. Heit JJ, Apelqvist AA, Gu X, et al. Calcineurin/NFAT signalling regulates pancreatic beta-cell growth and function. Nature 2006; 443: 345–349.
29. Zhang N, Su D, Qu S, et al. Sirolimus is associated with reduced islet engraftment and impaired beta-cell function. Diabetes 2006; 55: 2429–2436.
30. Bell E, Cao X, Moibi JA, et al. Rapamycin has a deleterious effect on MIN-6 cells and rat and human islets. Diabetes 2003; 52: 2731–2739.
31. Lopez-Talavera JC, Garcia-Ocaña A, Sipula I, et al. Hepatocyte growth factor gene therapy for pancreatic islets in diabetes: Reducing the minimal islet transplant mass required in a glucocorticoid-free rat model of allogeneic portal vein islet transplantation. Endocrinology 2004; 145: 467–474.
32. Cantaluppi V, Biancone L, Romanazzi GM, et al. Antiangiogenic and immunomodulatory effects of rapamycin on islet endothelium: Relevance for islet transplantation. Am J Transplant 2006; 6: 2601–2611.
33. Miriuka SG, Rao V, Peterson M, et al. mTOR inhibition induces endothelial progenitor cell death. Am J Transplant 2006; 6: 2069–2079.
34. Zahr E, Molano RD, Pileggi A, et al. Rapamycin impairs *in vivo* proliferation of islet beta-cells. Transplantation 2007; 84: 1576–1583.
35. Li X, Zhang L, Meshinchi S, et al. Islet microvasculature in islet hyperplasia and failure in a model of type 2 diabetes. Diabetes 2006; 55: 2965–2973.
36. Mizushima N, Yamamoto A, Matsui M, et al. *In vivo* analysis of autophagy in response to nutrient starvation using transgenic mice expressing a fluorescent autophagosome marker. Mol Biol Cell 2004; 15: 1101–1111.
37. Johnson AL, Ratajczak C, Haugen MJ, et al. Tumor necrosis factor-related apoptosis inducing ligand expression and activity in hen granulosa cells. Reproduction 2007; 133: 609–616.
38. Ichii H, Pileggi A, Molano RD, et al. Rescue purification maximizes the use of human islet preparations for transplantation. Am J Transplant 2005; 5: 21–30.
39. Ichii H, Wang X, Messinger S, et al. Improved human islet isolation using nicotinamide. Am J Transplant 2006; 6: 2060–2068.
40. Sawada T, Matsumoto I, Nakano M, et al. Improved islet yield and function with ductal injection of University of Wisconsin solution before pancreas preservation. Transplantation 2003; 75: 1965–1969.
41. Andrikopoulos S, Blair AR, Deluca N, Fam BC, Proietto J. Evaluating the glucose tolerance test in mice. Am J Physiol Endocrinol Metab 2008; 295: E1323–E1332.
42. Laugharne M, Cross S, Richards S, et al. Sirolimus toxicity and vascular endothelial growth factor release from islet and renal cell lines. Transplantation 2007; 83: 1635–1638.
43. Jung HS, Chung KW, Won Kim J, et al. Loss of autophagy diminishes pancreatic beta cell mass and function with resultant hyperglycemia. Cell Metab 2008; 8: 318–324.
44. Ebato C, Uchida T, Arakawa M, et al. Autophagy is important in islet homeostasis and compensatory increase of beta cell mass in response to high-fat diet. Cell Metab 2008; 8: 325–332.
45. Mariño G, Salvador-Montoliu N, Fueyo A, et al. Tissue-specific autophagy alterations and increased tumorigenesis in mice deficient in Atg4C/autophagin-3. J Biol Chem 2007; 282: 18573–18583.
46. Fujitani Y, Kawamori R, Watada H. The role of autophagy in pancreatic beta-cell and diabetes. Autophagy 2009; 5: 280–282.
47. Coux O, Tanaka K, Goldberg AL. Structure and functions of the 20S and 26S proteasomes. Annu Rev Biochem 1996; 65: 801–847.
48. Masini M, Bugliani M, Lupi R, et al. Autophagy in human type 2 diabetes pancreatic beta cells. Diabetologia 2009; 52: 1083–1086.
49. Shintani T, Klionsky DJ. Autophagy in health and disease: A double-edged sword. Science 2004; 306: 990–995.
50. Fujitani Y, Ueno T, Watada H. Autophagy in health and disease. 4. The role of pancreatic beta-cell autophagy in health and diabetes. Am J Physiol Cell Physiol 2010; 299: C1–C6.
51. Marsh BJ, Soden C, Alarcón C, et al. Regulated autophagy controls hormone content in secretory-deficient pancreatic endocrine beta-cells. Mol Endocrinol 2007; 21: 2255–2269.

52. Moretti L, Cha YI, Niermann KJ, Lu B. Switch between apoptosis and autophagy: Radiation-induced endoplasmic reticulum stress? Cell Cycle 2007; 6: 793–798.
53. Maiuri MC, Zalckvar E, Kimchi A, Kroemer G. Self-eating and self-killing: Crosstalk between autophagy and apoptosis. Nat Rev Mol Cell Biol 2007; 8: 741–752.
54. Marchetti P, Masini M. Autophagy and the pancreatic beta-cell in human type 2 diabetes. Autophagy 2009; 5: 1055–1066.
55. Liu JJ, Lin M, Yu JY, Liu B, Bao JK. Targeting apoptotic and autophagic pathways for cancer therapeutics. Cancer Lett 2011; 300: 105–114.

Supporting Information

Additional Supporting Information may be found in the online version of this article.

Supplementary Materials and Methods

Please note: Wiley-Blackwell is not responsible for the content or functionality of any supporting materials supplied by the authors. Any queries (other than missing material) should be directed to the corresponding author for the article.

Dig Dis Sci (2012) 57:1238–1246
DOI 10.1007/s10620-011-1986-2

ORIGINAL ARTICLE

Mapping Analysis of Ghrelin Producing Cells in the Human Stomach Associated with Chronic Gastritis and Early Cancers

Shuji Takiguchi · Shinichi Adachi · Kazuyoshi Yamamoto · Eiichi Morii · Hiroshi Miyata · Kiyokazu Nakajima · Makoto Yamasaki · Kenji Kangawa · Masaki Mori · Yuichiro Doki

Received: 25 July 2011 / Accepted: 11 November 2011 / Published online: 7 December 2011

Abstract
Objective The majority of ghrelin producing cells (GPC) are present in the fundic gland of the stomach and recognized as X/A like cells. The detailed distribution of GPC in the stomach is still unknown in healthy and pathological subjects.
Methods We investigated the detailed distribution of GPC in the stomach, especially in relation with chronic gastritis, using surgical specimens from 12 patients with early gastric cancer. Either the anterior or posterior half of the whole stomach, which was a counterpart of the tumor bearing side, was subjected for immunohistochemistry of ghrelin, and the number of total GPC were semi quantitatively evaluated as GPC score. GPC score was compared with the degree of chronic gastritis, serum ghrelin concentration and body weight.
Results GPC was not observed in the pyloric gland, but heterogeneously distributed in the fundic gland mainly in upper body and the greater curvature. The GPC score showed about nine-fold difference, which correlated well with the degree of chronic gastritis by Sydney score ($r = -0.84$, $P < 0.001$). The serum ghrelin concentration was basically determined by the GPC score ($r = 0.75$, $P = 0.0047$); however, the obese patients showed low serum ghrelin concentration in spite of the presence of abundant GPCs. In the low GPC score patients, serum ghrelin was constantly low regardless of their body weight.
Conclusions GPC was inversely correlated with progression of chronic gastritis. Its quantification using immunohistochemistry of the whole stomach was useful to comprehensively evaluate ghrelin profile.

Keywords Ghrelin · Chronic gastritis · Gastric cancer · Immunohistochemistry

S. Takiguchi · S. Adachi · K. Yamamoto · H. Miyata · K. Nakajima · M. Yamasaki · M. Mori · Y. Doki (✉)
Department of Gastroenterological Surgery, Graduate School of Medicine, Osaka University, 2-2-E2 Yamadaoka, Suita, Osaka 565-0871, Japan
e-mail: ydoki@gesurg.med.osaka-u.ac.jp

E. Morii
Department of Pathology, Graduate School of Medicine, Osaka University, Osaka, Japan

K. Kangawa
Department of Biochemistry, National Cardiovascular Center Research Institute, Osaka, Japan

Introduction

The 28-amino-acid peptide, ghrelin, is isolated from rat and human stomach [1]. This peptide is an endogenous ligand for the growth hormone secretagogue receptor 1a (GHS-R1a), and stimulates growth hormone release from the pituitary gland. Ghrelin has been reported to function not only in the control of growth hormone secretion but also in the regulation of food intake and energy metabolism [2]. The function of ghrelin is to stimulate the appetite signal in the hypothalamus and gastrointestinal activity, such as peristalsis, gastric acid secretion, and pancreatic excretion, through the vagal nerve [3].

The majority of ghrelin is produced in the stomach and a smaller amount is secreted from other organs, such as intestine, pancreas, kidney, and hypothalamus [4, 5]. Therefore, circulating ghrelin levels decreased to 10–20% of the preoperative level immediately after total gastrectomy [6, 7]. By the histological examination, ghrelin producing cells (GPC) were immunohistochemically identified in the fundic glands, which had been regarded as X/A-like

cells [4]. X/A-like cells were named as they morphologically resemble pancreatic A-cells (glucagon producing cell), therefore considered as a kind of neuroendocrine cell. X/A-like cells are abundant next to histamine producing cells as endocrine cells in the stomach [4, 8], but the product had been unknown for a long time. There were few studies concerning distribution of GPC in human stomach including one using three autopsy patients [4] and another investigated only the lesser curvature of the stomach [9]. Other studies investigating the relationship between GPC and clinicopathological features used endoscopic biopsy samples [10, 11]. Thus, the detailed distribution of GPC in the stomach is still unknown in healthy and pathological subjects.

The circulating ghrelin level is greatly varied by diurnal rhythm, food intake and body weight in healthy individuals [12, 13]. Among various pathological status that affect circulating ghrelin level, the chronic gastritis caused by *Helicobacter pylori* (*H. pylori*) infection is the most commonly observed [14, 15]; its prevalence is estimated in more than 70% of Japanese people aged 50 and over [16]. Chronic gastritis by *H. pylori* is well-known to be a causative condition for gastric cancers, which is the most common malignant tumor in the Eastern countries [17]. Moreover, *H. pylori* infection should be a clue to explain the huge difference of nutritional status between Western and Eastern countries. Clinical observation suggests some symptoms of chronic gastritis, such as appetite loss, delayed gastric emptying and malnutrition, should be caused by ghrelin and GPC reduction. A few studies have reported that GPC is decreased in the chronic gastritis patients [10, 11]. However, the detailed relationship is still unclear since those studies have used only few endoscopic biopsy samples for the evaluation. The degree of chronic gastritis, probably that of GPC as well, is heterogeneous, therefore it is necessary for precise evaluation to analyze the whole gastric specimen. Thus, we investigated the detailed distribution of GPC and its association with chronic gastritis using human whole stomach, which were surgically removed due to early gastric cancers. This is the first study of precise mapping analysis of GPC in the human stomach and should help to understand the association of chronic gastritis and ghrelin.

Materials and Methods

Patients and Gastric Specimens

Twelve patients who underwent total gastrectomy due to early gastric cancer at Osaka University Hospital between September 2007 and September 2009 were enrolled in the study. There were nine males and three females with average age of 64.5 years, ranging from 45 to 83 years. Average BMI was 24.1 kg/m^2 ranging from 19.3 to 28.3 kg/m^2. There were three patients medicated by hypertension and two patients by hyperlipidemia; however, those with serious co-morbidity or other cancers were excluded from this study. Gastric cancers of all 12 patients were less invasive (mucosal or submucosal), small (ranging 12–25 mm, median 21 cm in diameter), and localized in the posterior or anterior wall of the stomach, that is, tumors did not reach either the greater or lesser curvature of the stomach. Immediately after surgery, whole stomach was opened by greater curvature incision for observation, then fixed in 10% buffered formalin for three days. After fixation, the stomach was separated into two pieces as posterior and anterior wall by longitudinal incision at the lesser curvature. The tumor bearing side of the stomach was subjected to ordinary pathological examination and the tumor-free half was used for this study. The entire half of the stomach was sliced longitudinally in 8-mm steps, and then cut into 4-cm length pieces. All specimens were embedded in paraffin and used for hematoxylin and eosin (H&E) stain, Giemsa stain and immunohistochemistry. Blood samples collected before surgery and clinicopathological information from patients' charts were also subject for this study.

Atrophic changes in the gastric body on endoscopy were diagnosed on the basis of the atrophic area displaying discoloration with or without blood vessel transparency. The grade of atrophic gastritis was assessed endoscopically using the atrophic pattern system [18, 19]. This classification divides the extent of atrophy into closed type (C-type) and open type (O-type). The C-type indicates that the atrophic border remains on the lesser curvature of the stomach, while the O-type means that the atrophic border no longer exists on the lesser curvature but extends along the anterior and posterior walls of the stomach.

The study was approved by the Osaka University Ethics Committee, and all patients gave written informed consent before study entry in accordance with the Helsinki Declaration. The study was registered at UMIN (http://www.umin.ac.jp with clinical trial number UMIN000002902).

Immunohistochemistry of Ghrelin Producing Cells

Immunohistochemical staining of GPCs was performed with the streptavidin–biotin-peroxidase-complex method (Histofine® SAB-PO(R) Kit, Nichirei Biosciences Inc., Tokyo, Japan). The following steps were performed at room temperature unless otherwise specified. Paraffin-embedded specimens were sectioned at 4-μm thickness, deparaffinized and dehydrated. To enhance immunoreactivity of ghrelin, antigens were retrieved at 95°C for 40 min in citric acid buffer. After blocking of endogenous

peroxidase activity for 20 min with methanol containing 1% H_2O_2, the sections were reacted for 15 min with normal goat serum to prevent nonspecific binding. They were then incubated overnight with the Anti-Rat Ghrelin Polyclonal Antibody (Trans Genic Inc. Kumamoto, Japan) at 4°C. This anti-rat ghrelin antibody specifically recognizes the N-terminal fragment of ghrelin and is able to recognize both rat and human ghrelin [20, 21]. On the next day, the sections were washed in 0.01 M phosphate buffered saline (PBS) and incubated for 20 min with 10 μg/ml biotinylated goat anti-rabbit IgG antibody. After washing PBS, the sections were reincubated for 20 min with 100 μg/ml peroxidase-conjugated streptavidin and stained with 3, 3′-diaminobenzidine tetrahydrochloride in 0.05 M tris–HCl buffer containing H_2O_2. The sections were finally washed in PBS and counterstained with hematoxylin. Negative controls were treated identically without the primary antibody.

Semi-quantitative evaluation of GPCs was performed by counting GPC in the microscope. At 100× magnification, the field of microscope was adjusted to the gastric mucosa area and the number of GPC, which were clearly recognized as cells with small cytoplasm and dark brown staining, were counted. In each 4-cm length section, ten fields of mucosa area were randomly chosen and the average number of GPCs was recorded. According to the average number of GPC, each gastric section was classified as an 'extra rich area' (>40), 'rich area' (20–40), 'middle area' (1–20), and 'poor area' (<1). Due to the differences in the size of the stomach, the number of sections for each patient ranged from 37 to 70 (average 51.2) in each half stomach. To adjust for the size of the stomach, the number of sections of each classification was translated to the proportion area (%) of the entire half stomach. Finally, we established GPC score using an original calculating formula to evaluate the number of GPCs in each patient as follows;

GPC score = 70 × (extra rich area %) + 30 × (rich area %) + 10 × (middle area %) + 0.5 × (poor area %). Twelve patients were classified to high and low groups divided by the median GPC score.

Blood Sampling and Hormone Assay

Preoperative blood samples were collected from patients before breakfast after an overnight fast, transferred into chilled tubes, stored on ice during collection, centrifuged, separated as serum, and stored at −50°C until assay. Serum total ghrelin level was measured using an enzyme-linked immunosorbent assay-kit (Human Desacyl-Ghrelin ELISA- kit® and Human Active (acyl) -Ghrelin ELISA-kit®, Mitsubishi Kagaku Iatron Inc., Tokyo, Japan). Total serum ghrelin concentration was calculated as acyl-ghrelin concentration plus desacyl-ghrelin concentration. Serum gastrin levels were measured using RIA (Gastrin RIA kit® II, TFB Inc., Tokyo Japan), and serum pepsinogen (PG) I and II were measured using Chemiluminescent enzyme immunoassay (CLEIA) (LUMIPULSE Presto®, Fujirebio Inc., Tokyo, Japan). Subjects were screened on the basis of the following PG-test positive criteria: PG I level of less than 70 ng/mL and PG I/II ratio of less than 3.0. The cut-off point for atrophic gastritis and gastric cancer screening has been widely accepted in Japan.

Histopathological Examination of Gastritis

All sections of the entire half stomach were stained with H&E stain. One co-author of the pathologist (M.E.) who was unaware of the clinical information and laboratory data examined histopathological features of chronic gastritis according to the updated Sydney system [22]. In brief, five histological parameters including chronic inflammation (mononuclear cells), polymorphonuclear activity (neutrophils activity), glandular atrophy, intestinal metaplasia, and *H.pylori* density were scored semi-quantitatively from 0 to 3 (none, mild, moderate, or marked) then the sum of the score of the five parameters were used as the final score. The presence of *H. pylori* was confirmed by Giemsa staining of the representative six sections near the greater curvature of the corpus and antrum of the stomach by the same pathologist.

Quantitative mRNA Assay

Each three biopsy samples were collected from the fornix, the upper, the middle, and the lower stomach without obvious pathological change by the fiberscope in the representative patient (Case 2 in Fig. 2). They were immediately lysed in 175 ml of RNA lysis buffer (4 M GTC, 0.01 M Tris (pH7.5), 0.97% b-mercaptoethanol; Promega). RNA was extracted using the Promega SV Total RNA Isolation kit (Promega, Southampton, UK) following the protocol recommended by the manufacturers, and contaminating genomic DNA were removed by DNAse. RNA yield and purity were determined using a spectrophotometer at 260 and 280 nm. First strand cDNA synthesis was performed using RNase Reverse Transcriptase (GIBCO BRL, Paisley, UK).

Quantitative PCR was performed on a Roche Light Cycler system (Roche Molecular Biochemicals, Manheim, Germany). PCR reactions were carried out in a reaction mixture consisting of 5.0 ml reaction buffer and 2.0 mM MgCl2 (Biogene Ltd, Cambridge, UK), 1.0 ml of each primer (1 ng/ml), 2.5 ml of cDNA and 0.5 ml of Light Cycler DNA Master SYBR Green I (Roche Molecular Biochemicals). Protocol conditions consisted of

denaturation at 95°C for 15 s, followed by 40 cycles at 94°C for 1 s, 58°C for 10 s and 72°C for 15 s, followed by melting curve analysis. For analysis, quantitative amounts of ghrelin gene expression were standardized against the house-keeping gene b-actin, as previously described [23]. Quantitative data analysis was made possible by the use of ghrelin RNA from serially diluted gastric cDNA. A total of 10 ml of the reaction mixture were subsequently electrophoresed on a 1.6% agarose gel and visualized by ethidium bromide, using a 1 kb DNA ladder (GIBCO BRL) in order to estimate the band sizes. As a negative control for all the reactions, distilled water was used in place of cDNA. The RNA levels were expressed as a ratio, using "delta–delta method", for comparing relative expression results between treatments in real-time PCR. The primers used were Ghrelin: sense 59-TGA GCC CTG AAC ACC AGA GAG-39, antisense 59-AAA GCC AGA TGA GCG CTT CTA-39. The expected size for ghrelin is 327 bp; b actin: sense 59-AAG AGA GGC ATC CTC ACC CT-39, antisense 59-TAC ATG GCT GGG GTG TTG AA-39. The expected size for actin is 216 bp.

Statistical Analysis

Numerical values were expressed as mean ± standard deviation (SD) unless otherwise indicated. Differences in parameters between high and low groups were tested by Mann–Whitney's *U* test. The correlations among GPC score, BMI, and updated Sydney score with serum ghrelin levels were evaluated by Pearson's correlation coefficient test. A P value of <0.05 was considered statistically significant. StatView version 5.0 (SAS Institute, Inc, Cary, NC, USA) was used for statistical analysis.

Results

Distribution of Ghrelin Producing Cells and Its Scoring

The GPC in the stomach were small and round or spindle-shaped. GPC were abundant from the neck to the bottom in the fundic glands, but not observed in the foveolar epithelial cells, pyloric glands or intestinal metaplasia cells (Fig. 1). Half stomach, of either anterior or posterior wall, was prepared as 8-mm steps and 4-cm lengths of gastric sections on a slide glass, which were classified by the average number of GPC in the microscopic field as extra rich area (>40), rich area (20–40), middle area (1–20), or poor area (<1). Using this classification and proportion of each area, GPC score was calculated as representative of the sum total number of GPC for each patient. Mapping of GPC and GPC score

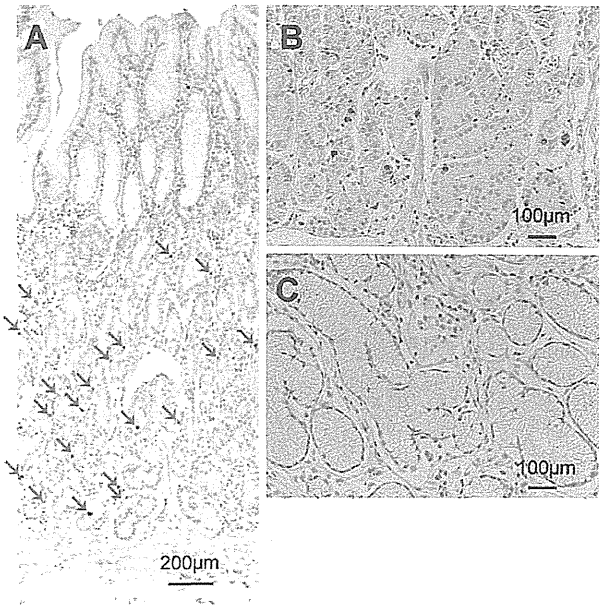

Fig. 1 Immunochemistry of ghrelin producing cells. Ghrelin producing cells (GPC) were stained by immunohistochemistry using anti ghrelin antibody. **a** Gastric mucosa in great curvature and corpus lesion showed GPC were not observed in the foveolar epithelial cells, but were abundant in the fundic glands (*arrows*) (×40). **b** Under higher magnification, GPC was recognized as small round or spindle cells with *brownish* stain in the cytoplasm (×400). **c** There were no GPC cells in the pyloric glands in the antrum (×400)

of 12 patients are shown in Fig. 2. GPC scores have shown approximately nine-fold differences among 12 patients ranging from 568 to 4511 (median 1472), and separated six patients into the high score group (median 2969; range 1791–4511) and six patients into the low score group (median 793; range 568–1153). It was a general trend that in the fundic gland area, GPC were more frequent in the greater curvature of the upper body and fornix and less frequent in the lesser curvature and anal and oral side. In the high score group, extra rich and rich areas tended to be dominant in the fundic gland area, while middle and poor areas were dominant in the low score group. Notably, some of the low score group (cases 7, 9, and 10), extra rich and/or rich area are still focally remaining.

Early gastric cancers which were small (size average 21 mm) and limited in the anterior or posterior wall were selected for this study. Gastric cancers were located in the anterior wall in two cases and posterior wall in ten cases, although the mapping image was inverted in the former in Fig. 2. None of cancer cells were positive for ghrelin immunohistochemistry. Symmetric distribution of GPC in the non-cancerous lesion was confirmed by comparing the number of GPC in the representative section located in the anterior and posterior walls of the upper body lesion (data not shown).

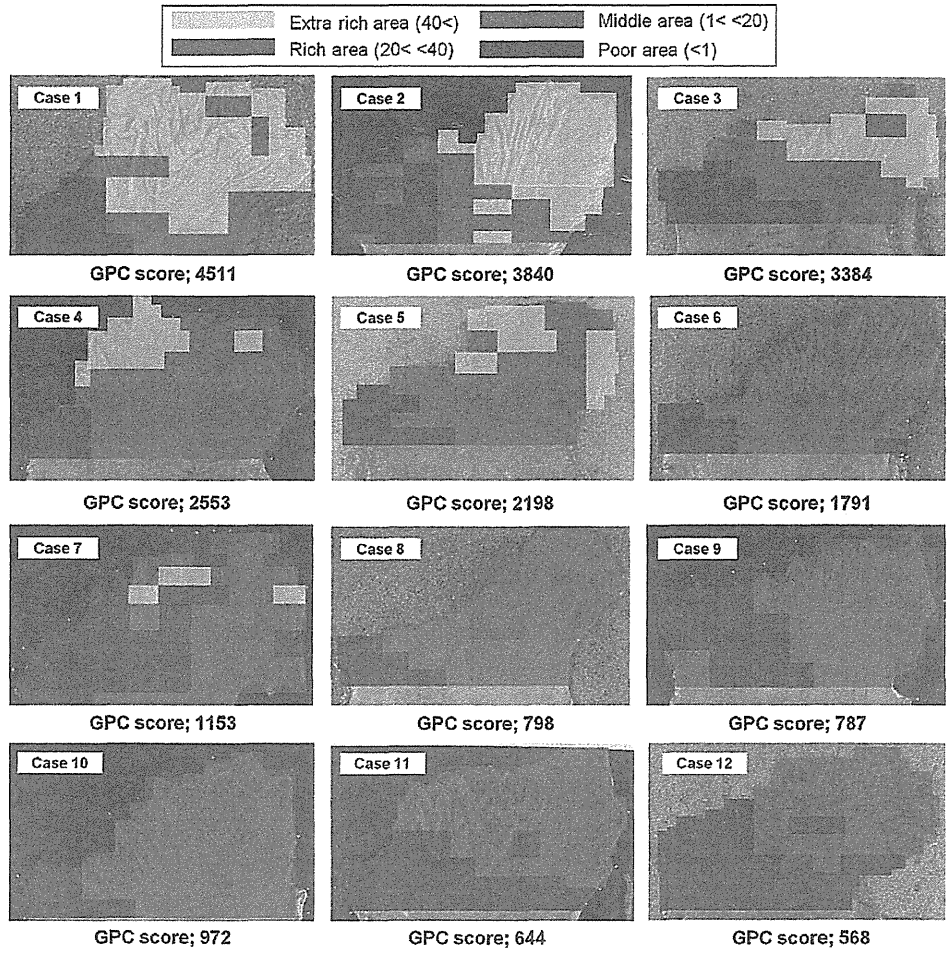

Fig. 2 Mapping of ghrelin producing cells (GPC) and GPC score of 12 patients. Half stomachs of 12 patients undergoing total gastrectomy due to early gastric cancers were subjected for GPC mapping. The number of GPC in each slide was classified as extra rich area (>40), rich area (20–40), middle area (1–20), or poor area (<1). Using this classification and proportion of each area, GPC score was calculated as representative of the sum total number of GPC for each patient. For cases 7 and 12, posterior half wall of the stomach was used for mapping and the image was inverted in this figure

GPC Score and Serum Ghrelin Levels

The average of serum total ghrelin levels was 65.7 ± 57.2 fmol/ml with large difference among patients ranging from 16.4 fmol/ml to 212.6 fmol/ml. There was a very strong and significant correlation among serum ghrelin levels and GPC score ($r = 0.75$, $P = 0.0047$, Fig. 3a). With respect to body weight, there was no correlation between BMI and GPC score ($r = 0.32$, $P = 0.31$, Fig. 3b). The inverse correlation between BMI and serum ghrelin, which was suggested in many previous studies, was not significant in this study ($r = -0.17$, $P = 0.60$, Fig. 3c). However, it is notable that in the GPC high score group, there was a trend that BMI showed negative correlation with serum ghrelin levels, while serum ghrelin levels were constantly low regardless of BMI in the low GPC score group (Fig. 3c). When focusing on two obese patients, serum ghrelin levels were relatively low despite high GPC score (arrows in Fig. 3a, b, c).

Chronic Gastritis and Ghrelin Feature

The degree of chronic gastritis was evaluated by updated Sydney System using H&E stained sections. As characteristic of early gastric cancer in Japan, ten of 12 patients showed moderate to severe chronic gastritis (Sydney score 5–10) and only two patients did not show significant gastritis less than 2 by updated Sydney score. In general, GPC was observed where fundic gland was preserved. However, we sometimes encountered absence of GPC in the fundic gland, where intestinal metaplasia and/or lymphocyte infiltration was prominent and thickness of fundic gland was declined.

There was significant inverse correlation of updated Sydney score with both GPC score and serum ghrelin, although the relationship was stronger with the former ($r = -0.84$, $P < 0.001$ and $r = -0.67$, $P = 0.016$, Fig. 4a, b). Besides updated Sydney score, various factors associated with chronic gastritis, including age, *H. pylori*

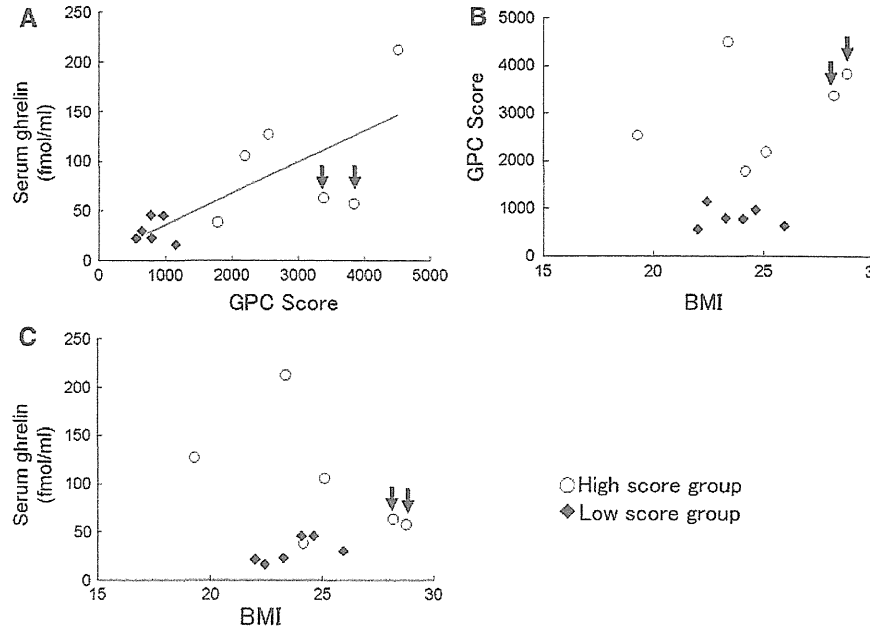

Fig. 3 The correlations among ghrelin producing cells (GPC) score, BMI, and serum ghrelin. Each two parameters among GPC score, BMI and serum total (acyl + des-acyl) ghrelin was plotted for 12 patients, who were classified as high (*open circle*) and low (*closed square*) GPC score. There was a significant correlation between serum ghrelin and GPC score ($r = 0.75$, $P = 0.0047$) (**a**), but BMI did not correlate with either GPC score ($r = 0.32$, $P = 0.31$) (**b**) or serum ghrelin ($r = -0.17$, $P = 0.60$) (**c**). Two patients with BMI greater than 28 were indicated by the *arrow*. They showed low serum ghrelin in spite of high GPC score

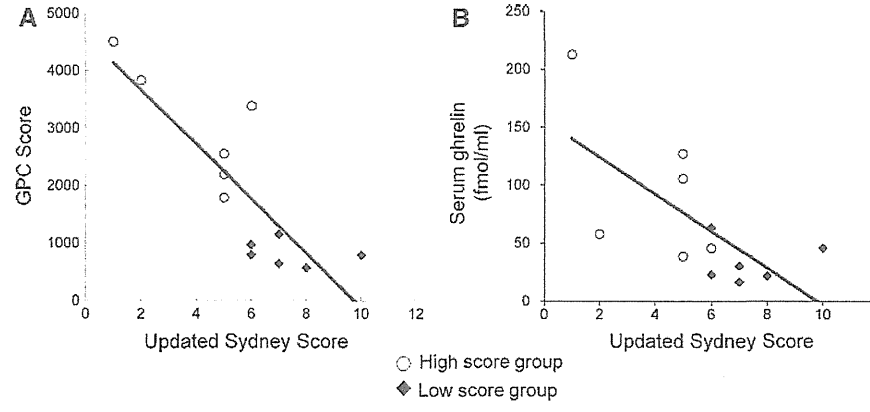

Fig. 4 The relationship between chronic gastritis and ghrelin profile. The degree of chronic gastritis was evaluated by updated Sydney score system, which was correlated with GPC score (**a**) and serum ghrelin (**b**). Patients were classified as high (*open circle*) and low (*closed square*) GPC score. Significant correlation was observed in both Fig. 5a ($r = -0.84$, $P < 0.001$) and 5b, ($r = -0.67$, $P = 0.016$)

infection, pepsinogen test and gastrin, were investigated for relationship with GPC score in Table 1. Age was not different between the two groups and females were more frequent in the high GPC group. Presence of *H. pylori* and pepsinogen positive test was more frequent and gastrin was higher in the GPC low group than in the GPC high group. With respect to histology of gastric cancer, intestinal type was more frequent in the GPC low group than in the GPC high group. However, these differences were not statistically significant due to a limited number of patients. When serum ghrelin was used for comparison instead of GPC score, serum ghrelin tended to be higher in females than in males (82.8 ± 39 vs. 60.0 ± 63, $P = 0.12$), in the *H. pylori* negative than in positive (106 ± 82 vs. 48.4 ± 28, $P = 0.27$) and in diffuse type than in intestinal type (101 ± 70 vs. 40.2 ± 31, respectively, $P = 0.019$). With respect to atrophic changes of gastric mucosa assessed by endoscopy, there were not significant associations between macroscopic mucosal change and GPC score.

Quantitative mRNA Assessment of Ghrelin Expression and the Number of Ghrelin Positive Cells

The quantitative mRNA of ghrelin expression was assessed from the biopsy samples by endoscopy before gastrectomy at each anatomical site of the stomach (Fig. 5a). The density of ghrelin-positive cells in gastric mucosa varied according to the anatomical site (Fig. 5b). The median number of ghrelin-positive cells at each anatomical section of mucosa was 74.5 in the fornix, 52 in the upper, 36 in the middle, and 23 in the lower stomach. There was an apparent correlation between ghrelin mRNA expression in gastric mucosa samples and ghrelin producing cell counts in immunohistochemistry ($R^2 = 0.87$, $P < 0.001$).

Table 1 Baseline characteristics

Parameter	Total	GPC score high group	GPC score low group	*P*
Age, median (year)	64.5 (45–83)	66.0 (54–74)	62.0 (45–83)	0.47[a]
Gender (male/female)	9/3	3/3	6/0	0.091[b]
BMI, median (kg/m^2)	24.1 (19.3–28.8)	24.6 (19.3–28.8)	23.7 (22.0–25.9)	0.50[a]
H. pylori infection (positive/negative)	8/4	3/3	5/1	0.27[b]
Pepsinogen test (positive/negative)	5/7	1/5	4/2	0.12[b]
Atrophic change (C-type/O-type)	5/7	2/4	3/3	0.56[b]
Gastric cancer differentiation (undiff/diff)	5/7	4/2	1/5	0.12[b]
Gastrin; median (pg/mL)	204 (95–630)	135 (95–240)	210 (100–630)	0.26[a]

[a] Mann–Whitney's *U* test

[b] Fisher's exact probability test

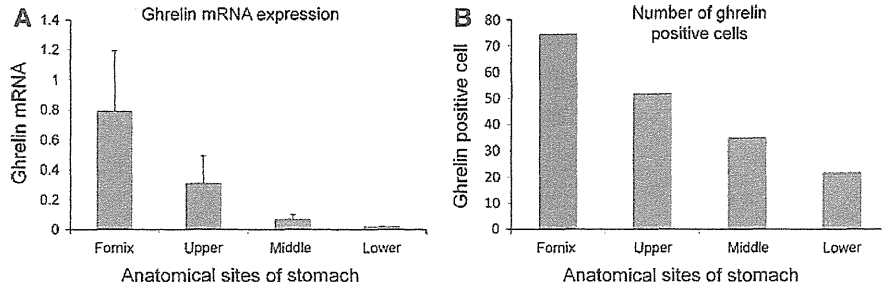

Fig. 5 Quantitative mRNA assessment of ghrelin expression and the number of ghrelin positive cells at each anatomical site of the stomach. The quantitative RT-PCR of ghrelin mRNA was assessed using the biopsy samples obtained by endoscopy at each site of the stomach (**a**). Ghrelin positive cells were counted by immunohistochemistry at each site of the stomach (**b**). There was an apparent correlation between ghrelin mRNA expression in gastric mucosa samples and ghrelin producing cell counts in immunohistochemistry ($R^2 = 0.87$, $P < 0.001$)

Discussion

This is the first study, which performed mapping and scoring of GPC in human subjects, focusing on the relationship between GPC and chronic gastritis using surgical samples of early gastric cancers. GPC has been known to be identical to the X/A-like cells in the fundic gland. Consistently, we observed GPC the most frequently in the great curvature in the upper body and fornix of the stomach where the fundic glands are well developed. Accompanying the progression of chronic gastritis, the number of GPC gradually decreased up to 10–20% of that without gastritis. The pattern of decline of GPC was various: some showed homogenous decrease of GPC in fundic gland area, but others showed heterogeneous or mosaic decrease, i.e. the GPC rich area was focally preserved. In general, GPC was well correlated with the preservation of fundic gland; however, we sometimes encountered the area where GPC was selectively lost despite when other components of fundic gland, such as chief cells and parietal cells, were present. Many clinical studies used endoscopic biopsy specimens for the evaluation of GPC. However, our observation might be a caution against these studies and we strongly recommend examining multiple specimens, at least one from the great curvature in the upper body and others from several lesions in fundic gland area.

The GPC score of the stomach was strongly correlated with serum ghrelin levels in the peripheral blood. This suggests the stomach is the main organ of ghrelin secretion and consistent with our previous observation that ghrelin has decreased to 10–20% after total gastrectomy [6, 7]. The current observation has also shown that the decline of GPC in the stomach was not compensated by the other ghrelin-producing organs, such as the duodenum, pancreas and hypothalamus, during the long history of chronic gastritis. With respect to the association with body weight, GPC score is not correlated with BMI, but serum ghrelin tends to negatively correlate with BMI in the GPC high group. This suggests the negative feedback that circulating ghrelin decrease in the obese individual was not by the regulation of GPC number but by that of the ghrelin secretion from GPC. GPC as well as serum ghrelin can be the surrogate marker of chronic gastritis like pepsinogen, gastrin and the presence of *H pylori*, while GPC might be more sensitive than serum ghrelin, since GPC is less influenced by body weight.

In this study, we used entire half stomach from patients with early gastric cancers, which should be good examples to investigate the relationship between chronic gastritis and ghrelin. The presence of cancer cells might not have much influence on GPC score and serum ghrelin levels, since the size of cancer nests was small and the GPC distribution was not perturbed in the mucosa surrounding the cancer nest. With respect to cancer cells, the high GPC group was associated with diffuse type cancers and low GPC group with intestinal type cancers. The association was considered due to the difference of background mucosa in each histological type. And it is unlikely that the ghrelin has a special effect on cancer progression. All the gastric cancer cells were negative for ghrelin immunohistochemistry in this study.

Ghrelin has acyl (active) and desacyl (inactive) forms and the active form accounts for 5.6–13% of total ghrelin [24]. Activation of ghrelin is conducted in the cytoplasm by ghrelin O-acyl transferase (GOAT), which is reported to co-exist with ghrelin in the stomach [25, 26]. However, the active form of ghrelin should be determined not only through the activation process by GOAT, but also through the inactivation by releasing the octanoyl-residue at Ser3 [24]. Ghrelin has a unique post-translational modification. The hydroxyl group of the third serine residue (Ser3) is esterified by octanoic acid and is essential for ghrelin's biological activities. The acyl modification of the hydroxyl group on the third residue represents an invariant and essential covalent change for the activation of ghrelin [24, 27]. Since the proportion of the active form varied among individuals and some conditions, it is quite interesting how the proportion of the active form and whether GOAT is constantly expressed in the GPC during the progression of chronic gastritis. We are planning further experiments with this issue.

Although this was an observational study with a small number of subjects, we can find important clues to resolve some surgical problems. Sleeve gastrectomy in bariatric surgery longitudinally removes the majority of the great curvature of the stomach. For successful body weight loss, not only gastric volume reduction but also appetite loss can be expected since the majority of GPC was removed by this procedure [28]. On the contrary, a gastric tube for reconstruction after esophagectomy was made of the great curvature of the stomach. Since body weight loss is a serious late complication after esophagectomy, preservation of the majority of GPC in the gastric tube might be beneficial to maintain the appetite. With respect to distal gastrectomy for gastric cancers, the majority of GPC should be anatomically preserved, but blood ghrelin decreases less than half [6, 7]. Vagotomy might be responsible for this discrepancy, therefore preservation of the vagal nerve might be worth attempting to maintain ghrelin and body weight.

Ghrelin, which plays a central role in the regulation of body weight and the appetite, should be a key molecule for studies of the various gastro-intestinal diseases, including chronic gastritis and morbid obesity. The precise distribution of GPC in the stomach is indispensable information for scientists and physicians and especially for the surgeon dealing with stomach.

Conclusion

This is the first study involving mapping of GPCs, which showed heterogenous impairment by chronic gastritis due to *H. pylori* infection. Since serum total ghrelin was mostly determined by the amount of GPCs and body weight, precise evaluation of GPCs should always be considered for the studies with respect to ghrelin.

Acknowledgments The authors thank Tomoyuki Sugimoto Ph.D. from the Department of Biomedical Statistics, Osaka University for advice on statistical analysis.

References

1. Kojima M, Hosoda H, Date Y, et al. Ghrelin is a growth-hormone-releasing acylated peptide from stomach. *Nature*. 1999;402:656–660.
2. Nakazato M, Murakami N, Date Y, et al. A role for ghrelin in the central regulation of feeding. *Nature*. 2001;409:194–198.
3. Masuda Y, Tanaka T, Inomata N, et al. Ghrelin stimulates gastric acid secretion and motility in rats. *Biochem Biophys Res Commun*. 2000;276:905–908.
4. Date Y, Kojima M, Nakazato M, et al. Ghrelin, a novel growth hormone-releasing acylated peptide, is synthesized in a distinct endocrine cell type in the gastrointestinal tracts of rats and humans. *Endocrinology*. 2000;141:4255–4261.
5. Leite-Moreira AF, Soares JB. Physiological, pathological and potential therapeutic roles of ghrelin. *Drug Discov Today*. 2007;12:276–288.
6. Takachi K, Doki Y, Ishikawa O, et al. Postoperative ghrelin levels and delayed recovery from body weight loss after distal or total gastrectomy. *J Surg Res*. 2006;130:1–7.
7. Doki Y, Takachi K, Ishikawa O, et al. Ghrelin reduction after esophageal substitution and its correlation to postoperative body weight loss in esophageal cancer patients. *Surgery*. 2006;139:797–805.
8. Simonsson M, Eriksson S, Håkanson R, et al. Endocrine cells in the human oxyntic mucosa. A histochemical study. *Scand J Gastroenterol*. 1988;23:1089–1099.
9. Shintani M, Watanabe M. Distribution of ghrelin-immunoreactive cells in human gastric mucosa: comparison with that of parietal cells. *J Gastroenterol*. 2005;40:345–349.
10. Osawa H, Nakazato M, Date Y, et al. Impaired production of gastric ghrelin in chronic gastritis associated with *Helicobacter pylori*. *J Clin Endocrinol Metab*. 2005;90:10–16.
11. Tatsuguchi A, Miyake K, Futagami S, et al. Effect of *Helicobacter pylori* on ghrelin expression in human gastric mucosa. *Am J Gastroenterol*. 2004;99:2121–2127.
12. Cummings DE, Weigle DS, Frayo RS, et al. Plasma ghrelin levels after diet-induced weight loss or gastric bypass surgery. *N Engl J Med*. 2002;346:1623–1630.
13. Ariyasu H, Takaya K, Tagami T, et al. Stomach is a major source of circulating ghrelin, and feeding state determines plasma

ghrelin-like immunoreactive levels in humans. *J Clin Endocrinol Metab.* 2001;86:4753–4758.
14. Isomoto H, Ueno H, Nishi Y, et al. Circulating ghrelin levels in patients with various upper gastrointestinal diseases. *Dig Dis Sci.* 2005;50:833.
15. Isomoto H, Ueno H, Saenko VA, et al. Impact of *Helicobacter pylori* infection on gastric and plasma ghrelin dynamics in humans. *Am J Gastroenterol.* 2005;100:1711–1720.
16. Inoue M, Tsugane S. Epidemiology of gastric cancer in Japan. *Postgrad Med J.* 2005;81:419–424.
17. Uemura N, Okamoto S, Yamamoto S, et al. Helicobacter pylori infection and the development of gastric cancer. *N Engl J Med.* 2001;345:784–789.
18. Kimura K, Takemoto T. An endoscopic recognition of the atrophic border and its significance in chronic gastritis. *Endoscopy.* 1969;3:87–97.
19. Kimura K, Satoh K, Ido K, et al. Gastritis in the Japanese stomach. *Scand J Gastroenterol Suppl.* 1996;214:17–20.
20. Hosoda H, Kojima M, Matsuo H, et al. Ghrelin and des-acyl ghrelin: two major forms of rat ghrelin peptide in gastrointestinal tissue. *Biochem Biophys Res Commun.* 2000;279:909–913.
21. Nagaya N, Kojima M, Uematsu M, et al. Hemodynamic and hormonal effects of human ghrelin in healthy volunteers. *Am J Physiol.* 2001;280:1483–1487.
22. Dixon MF, Genta RM, Yardley JH, et al. Classification and grading of gastritis. The updated Sydney System. International workshop on the histopathology of gastritis, Houston 1994. *Am J Surg Pathol.* 1996;20:1161–1181.
23. Gualillo O, Caminos J, Blanco M, et al. Ghrelin, a novel placental-derived hormone. *Endocrinology.* 2001;142:788–794.
24. Hosoda H, Kojima M, Kangawa K. Biological, physiological, and pharmacological aspects of ghrelin. *J Pharmacol Sci.* 2006;100:398–410.
25. Yang J, Brown MS, Liang G, et al. Identification of the acyltransferase the octanoylates ghrelin an appetite-stimulating peptide hormone. *Cell.* 2008;132:387–396.
26. Stengel A, Goebel M, Wang L, et al. Differential distribution of ghrelin-O-acyltransferase (GOAT) immunoreactive cells in the mouse and rat gastric oxyntic mucosa. *Biochem Biophys Res Commun.* 2010;392:67–71.
27. Kaiya H, Kojima M, Hosoda H, et al. Bullfrog ghrelin is modified by n-octanoic acid at its third threonine residue. *J Biol Chem.* 2001;276:40441–40448.
28. Karamanakos SN, Vagenas K, Kalfarentzos F, et al. Weight loss, appetite suppression, and changes in fasting and postprandial ghrelin and peptide-YY levels after Roux-en-Y gastric bypass and sleeve gastrectomy: a prospective, double blind study. *Ann Surg.* 2008;247:401–407.